Biochimica et Biophysica Acta 1817 (2012) 552–557

Contents lists available at ScienceDirect

Biochimica et Biophysica Acta

journal homepage: www.elsevier.com/locate/bbabio

The origin of the $Fe^{IV}=O$ intermediates in cytochrome aa_3 oxidase ☆

Eftychia Pinakoulaki [a,1], Vangelis Daskalakis [b,1], Constantinos Varotsis [b,*,1]

[a] Department of Chemistry, University of Cyprus, P.O. BOX 20537, 1678 Nicosia, Cyprus
[b] Department of Environmental Science and Technology, Cyprus University of Technology, P.O. Box 50329, 3603 Lemesos, Cyprus

ARTICLE INFO

Article history:
Received 3 June 2011
Received in revised form 18 July 2011
Accepted 19 July 2011
Available online 26 July 2011

Keywords:
Heme–copper oxidase
Ferryl intermediate
Resonance Raman spectroscopy
Molecular dynamics simulation

ABSTRACT

The dioxygen reduction mechanism in cytochrome oxidases relies on proton control of the electron transfer events that drive the process. Proton delivery and proton channels in the protein that are relevant to substrate reduction and proton pumping are considered, and the current status of this area is summarized. We propose a mechanism in which the coupling of the oxygen reduction chemistry to proton translocation (P→F transition) is related to the properties of two groups of highly conserved residues, namely, His411/G386-T389 and the heme a_3–propionateA–D399–H403 chain. This article is part of a Special Issue entitled: Respiratory Oxidases.

1. Introduction

The superfamily of heme–copper oxidoreductases consists of three distinct families (A, B, and C families) which couple the redox chemistry to proton pumping [1–3]. Cytochrome *c* oxidase (CcO) uses four redox-active metal centers, Cu_A, heme *a*, and the heme a_3–Cu_B binuclear center, to sustain electron transport by reducing oxygen to water. CcO couples the one-electron oxidation of cytochrome *c* to the four-electron reduction of molecular oxygen and links these electron transfers to proton translocation. Rather than dissipate the free energy of the O_2 reaction as heat, a mechanism has evolved that allow oxidases to use the free energy made available to pump protons against their chemiosmotic gradient, thereby contributing directly to $\Delta\mu_{H+}$. Establishing the functional and structural properties of transient O_2 intermediates, the electron and proton transfer pathways, the loading and exit proton channels in CcO is essential in understanding the linkage of these events with proton translocation.

A considerable amount of effort has been devoted to understanding the coupling of the dioxygen reduction to proton translocation [1–3]. Beginning with the oxidized enzyme form of the enzyme, indicated as a hydroxyl species, two electrons are delivered from cytochrome *c* through Cu_A and heme *a* cofactors of the enzyme to the binuclear heme a_3–Cu_B center. These electron transfers produce the ferrous/cuprous reduced form of the active site, which binds O_2 to yield the initial oxy intermediate. Subsequent intra- and intermolecular electron and proton transfer generates the P and F intermediates that are ultimately converted back to the hydroxyl form to initiate additional cycles of the dioxygen-reducing/proton-pumping process. The proton control reduction of O_2 by oxidase has a number of important consequences. Therefore, establishing the structures of the intermediates prior and subsequent to the O–O bond cleavage is essential in understanding the linkage of these events to proton translocation.

2. The origin of the 607/580-nm forms and the resonance Raman assignments of the ferryl intermediates

CcO catalyzes several different reactions with O_2 and H_2O_2 that share some or all intermediate steps. A number of reactions intermediates have been identified in both reactions [4–9]. The CcO/H_2O_2 reaction serves as an alternative view of the peroxy ($2e^-$) oxidation level. The CcO/H_2O_2 reaction, monitored extensively by optical spectroscopy, forms consequently the 607- and 580-nm forms, and their formation is dependent on pH and the concentration of substrate. Stoichiometric amounts of H_2O_2 to oxidize enzyme at high pH lead to the formation of the 607 nm species (P intermediate), which is subsequently protonated to form the 580 nm species (F intermediate). On the other hand, at low-pH, the 580 nm species can be also produced by addition of stoichiometric amounts of H_2O_2. Based on resonance Raman experiments in the pH 7.4–10 range the population of the 607-nm species with a characteristic ν(Fe(IV)=O mode at 804 cm^{-1} decreases at high pH and at high concentrations of H_2O_2. The formation of the 580 nm form at non-saturation levels of substrate, yields two distinct oxygen sensitive vibrations at 785 and 355 cm^{-1}. Recently, it was reported that the pK_a of the 607 to 580 nm transition is 7.5, and based on the high frequency resonance Raman data (Fig. 1) the formation of six-coordinate low spin species at high and low pH, excludes the formation of a porpyrin π-cation radical [9]. We also observed three oxygen isotope-sensitive Raman

☆ This article is part of a Special Issue entitled: Respiratory Oxidases.
* Corresponding author. Tel.: +357 25002451; fax: +357 25002802.
E-mail address: c.varotsis@cut.ac.cy (C. Varotsis).
[1] All authors have contributed equally to this work.

0005-2728/$ – see front matter © 2011 Elsevier B.V. All rights reserved.
doi:10.1016/j.bbabio.2011.07.009

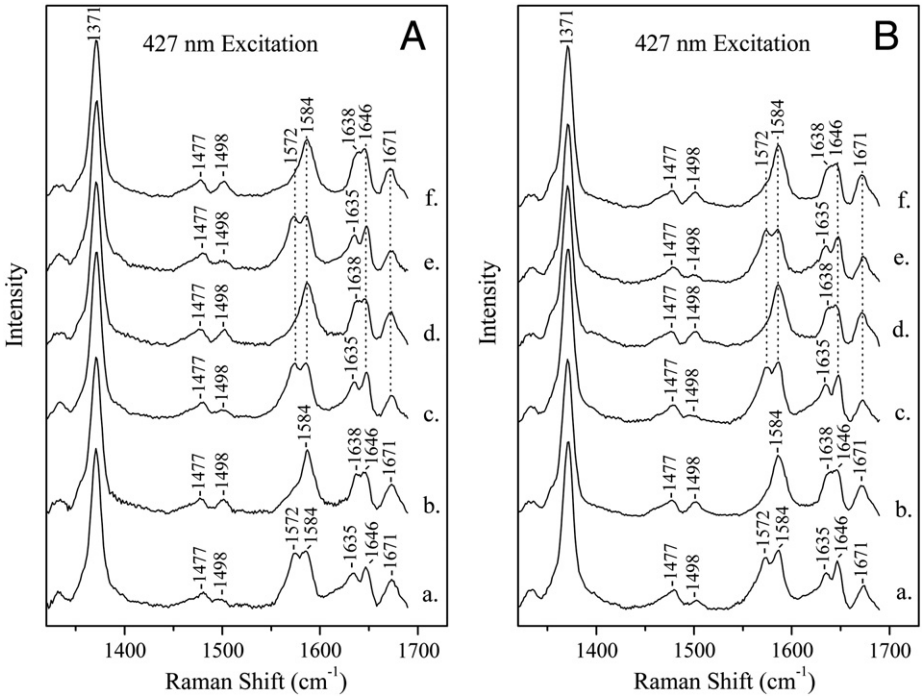

Fig. 1. High frequency resonance Raman spectra of wild type cytochrome aa_3 from *P. denitrificans* and those of the reaction intermediates with H_2O_2 at 2 min subsequent to mixing. Panel A: Trace a, pH 6.6; trace b, the reaction product at pH 6.6; trace c, pH 7.7; trace d, the reaction product at pH 7.7; trace e, pH 9.6; trace f, the reaction product at pH 9.6. Panel B: Trace a, pD 6.6; trace b, the reaction product at pD 6.6; trace c, pD 7.7; trace d, the reaction product at pD 7.7; trace e, pD 9.6; trace f, the reaction product at pD 9.6. The concentration of the enzymes was 50 μM, and that of H_2O_2 was 3 mM. The excitation laser wavelength was 427 nm, and the incident laser power was 5–6 mW. The total accumulation time was 15 min for each spectrum. The RR spectra of the oxidized enzyme at pH 6.6, 7.7 and 9.6 are almost identical indicating that no unusual pH effects modify either the oxidation state of heme *a* and a_3 or the heme a_3 ligand binding site. The disappearance of the high spin ν_2 at 1572 cm^{-1} and ν_{10} at 1612 cm^{-1} during the reaction indicates the formation of oxygenated species similar to those reported for the bovine aa_3/H_2O_2. The absence of ν_2 and ν_{10} at those lower frequencies provide evidence against the formation of π-cation radical (positively charged radical). The radical is the result of oxidation of the porphyrin ring.

bands in the oxidized wild type aa_3/H_2O_2 reaction at 804, 790 and 358 cm^{-1}[9]. The former two were assigned to the Fe(IV = O) stretching mode of the 607 nm, P intermediate and 580 nm, F intermediates. In addition the 358 cm^{-1} mode was found to appear with the 804 cm^{-1} mode and was assigned as the bending δ(Fe(IV) = O) of the P intermediate. The 14 cm^{-1} frequency difference between the oxoferryl species was attributed to the variations in the basicity of the proximal to heme a_3 His-411, induced by the oxoferryl conformations of the heme a_3–Cu_B pocket during the 607–580 nm transition. It should be mentioned that the properties of the ferryl intermediates in the CcO/O_2 and CcO/H_2O_2 reaction that appear in the 785–805 cm^{-1} frequency range are complicated, and several interpretations have been reported [4–9].

Both electronic and structural factors are expected to contribute to the differences between the 607 and 580 species in absorption maxima. The most likely rationale for the conversion of the 607- to 580-nm form is the hydrogen-bonding differences in the distal environment and variations in the proximal to heme a_3 H411 basicity. The large difference, ~25–30 nm, between the two forms argues against the interpretation that a single change in H-bonding of the bound heme a_3 Fe(IV) = O will shift the absorption spectrum by at least 25 nm. It has been demonstrated, however, that a shift of 7 nm in the optical spectrum results from an H-bonded relative to a non-H-bonded Fe(IV) = O species [10]. We suggest that a change in the distal H-bonded environment of the oxoferryl species can be communicated to the proximal environment causing a modification of the H-bonding status of the proximal heme a_3–His. This way, the optical transition will shift to higher energy as a result of the increased splitting of the d orbitals and the energy of the antibonding π* orbitals. The data for the aa_3-type oxidase from *Bacillus subtilis* [11] show that such heme-linked ionisation phenomena exist in heme–copper oxidases, and support our interpretation that the effect comes from the unique interactions between the distal heme pocket and coordinated oxo that are communicated to the proximal environment causing perturbations in the H-bonding interactions of H411(see below).

The vibrational properties of oxygenated intermediates in histidine-containing peroxidase catalysis have been explained by the push–pull reaction mechanism [12,13]. It involves the distal histidine that acts as a base to accelerate the binding of H_2O_2 by deprotonating the substrate generating a Fe^{3+}–O–O–R species. The pull aspect of the mechanism is completed by donation of a proton to the terminal oxygen of the hydroperoxide by the same residue acting as an acid. Concurrently, in the push component of the mechanism an amino acid in the proximal pocket hydrogen bonds to the proximal histidine and imparts significant anionic character to this residue. It is well known from RR studies that the properties of the trans ligand of oxoferryl complexes can affect the bonding between the Fe and the O, and thus its vibrational frequency [14]. Similarly, the basicity of the proximal H411 can be significantly enhanced by local protein forces and can explain the observed structural differences between the two oxoferryl species we observe at 790 and 804 cm^{-1}. Based on the crystal structure the proximal H411 is capable of forming hydrogen bonds with G386 and T389. A high Fe–His mode arises from a population in which the hydrogen bond is intact, whereas a lower Fe–His vibration reflects a form of the enzyme lacking the hydrogen bond. In the presence of an H-bonded H411, electron density is pushed into the antibonding π* orbitals of Fe(IV) = O weakening the bond and thus shifting the Fe(IV) = O stretching frequency from 804 to 790 cm^{-1}. We postulate that conformational changes of the bound oxo ligand by the heme a_3/Cu_B pocket are communicated to the proximal environment to facilitate the H-/non-H-bonding interaction of the proximal H411. It is tempting to propose that although the H-bonding interaction of T389 and G386 with the proximal His 411 alone is sufficient to cause the 14 cm^{-1} variation, the neutralization of the negatively charged propionate groups on the heme could modulate

the electron density in a manner similar to electron-withdrawing substituents.

The data from the ferryl intermediates may be discussed in the framework of proton motion. The details of how the 804 to 790 cm^{-1} oxoferryl transition is specifically tuned to initiate proton motion are reported here. In addition, the specific properties of the ferryl intermediates investigated in this work include: a) the bond strength and constrains of the proximal His411 residue, b) the presence of H-bonding distal residues in the binding heme a_3–Cu_B binuclear center and c) the H-bonding between the conserved D399–H403 and the propionate A of heme a_3. Our data provide insight into these interactions and provide tentative mechanism for the P–F transition. We postulate that there is a conformational change at the distal site of the binuclear center when the 607 to 580 nm transition occurs that is communicated to the proximal site of heme a_3 resulting in H-bonding perturbation of the proximal to heme a_3 H411. The 607 to 580 nm transition may also induce a protonic connectivity between the heme a_3–propionates–Asp–H_2O. This way the state of protonation of the proximal histidine and that of the heme a_3–propionates–Asp–H_2O chain is controlled by the redox events of the heme a_3/Cu_B binuclear center. Importantly, the protonic connectivity of the latter group has been recently reported in cytochrome ba_3 from *Thermus thermophilus* [15–17]. Therefore, in this proposed mechanism the coupling of the oxygen reduction chemistry to proton translocation (P→F transition) is related to the properties of two groups of central elements, namely, His411/G386–T389, the heme a_3–propionateA–D399–H403–H_2O chain and the H-bonding between the conserved D399–H403 and the propionate A of heme a_3.

3. Proton transfer mechanisms

It has been recently proposed that the transfer of a proton (H^+) from E278 (*Paracoccus denitrificans* numbering) to an unknown residue above the hemes a/a_3 is the first step in the pumping mechanism by CcO across the mitochondrial membrane. During P→F transition, E278 is protonated via the D-pathway, its proton is then transferred to the active site and E278 is re-protonated, while a proton is released to the P-side [18].

The 804/790 cm^{-1} ν(Fe–O) modes in the resonance Raman spectra have been theoretically attributed to the same oxidation level with oxo–ferryl character in the CcO dioxygen reaction [19]. The protonation state of the prop-A/Asp399 pair seems not to influence significantly the location of the 804/790 cm^{-1} bands but only their intensities. Thus, different protonated/deprotonated states of this pair vary the intensity of one band over the other. This results in the appearance of one or two prominent positive bands in the difference spectra of isotopically substituted species such as the ferryl–oxo intermediates in the CcO dioxygen reaction [20]. Moreover, for the enhancement of the δ(His–Fe=O) ferryl bending mode, we have identified crucial resonances, and we link them to conformational/structural changes during enzymatic turnover, including the Fe–Cu_B distance controlled by electrostatic interactions in the active site and especially in the area of the propionates [21]. More precisely, the position of Cu_B closer to or away from the heme a_3 plane appears sensitive also to the protonation events in the propionates. In addition, the conformational changes in the region of the ring A propionate of heme a_3, due to protonation events, are communicated via Asp399/His403 to Gly386/Thr389 in the proximal area altering H-bonding networks in the region. This, in turn, controls the proximal ligand effect of the His411 on the ν(Fe–O) mode.

A theoretical proof for the direct link between the D-pathway and the water pool has been achieved at the QM/MM level of theory. Two proton valves (E278 and His403) and an electron/proton coupling site (prop-A/Asp399) exist in this pathway. His403 is able to change its conformation enabling or disabling the release of a proton from the active site. His403 is able to control the protonation state of the prop-A/Asp399 pair, while it is coordinated to the Mg site near the *water pool*. Being strategically placed at the water exit in the CcO active site, its conformation interacts with the water molecules on their way to the *water pool* [21].

3.1. Bond strength correlations

As key residues and sites have been identified in the CcO active site, which serves as possible proton carriers, valves and electron–proton couplers, it is important to observe the correlation between different atomic distances between such sites. Correlation of bond distances in the active site of CcO, as well as the ν(Fe–O) mode, appears in Fig. 2 for the ferryl intermediate, based on average bond distances and FFT (Fast-Fourier Transform) derived ν(Fe–O) modes from Molecular Dynamics simulations [19]. We can observe that the protonation state of the prop-A/Asp399 pair controls a) the H-bonding interactions of the proximal His411 and b) the Fe–N(His411) distance. In Fig. 2A we can also observe a dependence of the Fe_{a3}–Cu_B distance on the protonation state of prop-A/Asp399 pair. The protonation state of the latter pair changes with

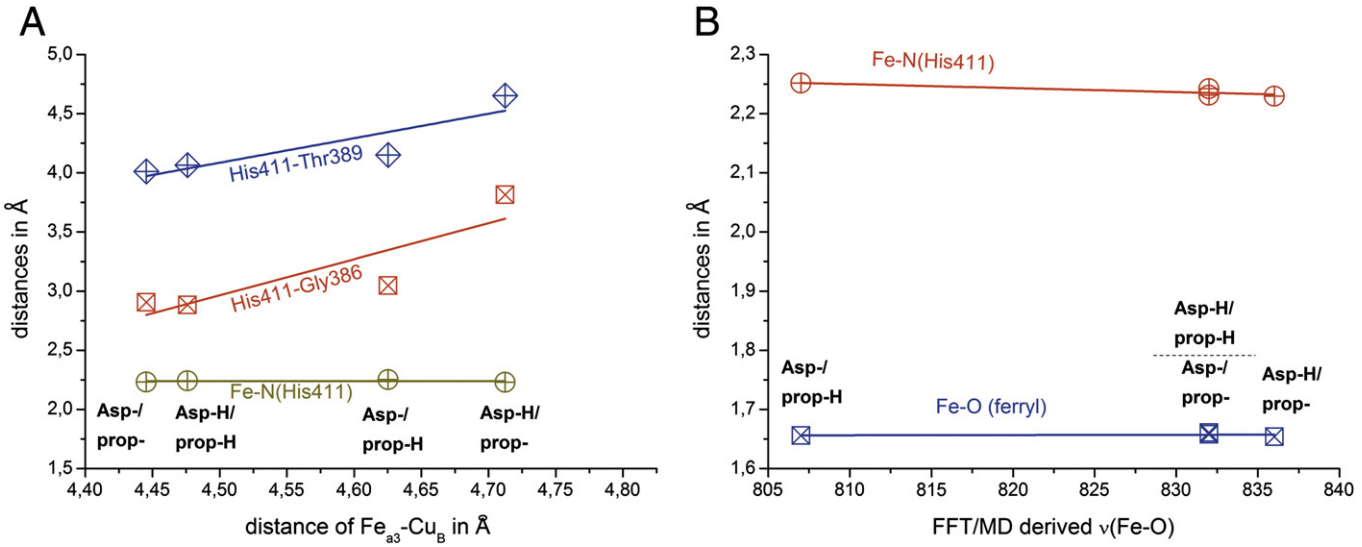

Fig. 2. Correlation diagrams depicting: A. the interactions of His411 in the proximal area and how these affect the His411–Thr389/Gly386, Fe–N(His411) and Fe_{a3}–Cu_B atomic distances when the protonation state of the propionate A (prop-A)/Asp399 pair is varied. B. the effect of the variation in Fe^{IV}=O (ferryl) and Fe–N(His411) bond lengths on the ν(Fe=O) mode.

direct effect on the hydrogen bonding interactions in the proximal site. As hydrogen bonding to the proximal site (His411) increases in strength (Gly386–His411 and Thr389–His411 distances become shorter), the (His411)N–Fe bond becomes longer, while the Fe_{a3}–Cu_B distance shortens. In Fig. 2B we see a clear trend for the ν(Fe–O) which increases as the (His411)N–Fe bond becomes stronger.

3.2. Mechanism of action

Based on the theoretical results of the QM, MD and QM/MM calculations, we have designed a schematic overview of a proposed mechanism for proton/electron coupling. This is depicted in steps in Fig. 3:

A. It has been proposed that water molecules are present in the hydrophobic cavity near Glu278, connecting it to the heme a_3 propionate-D (prop-D) and Cu_B [23–26]. In this line, Glu278 undertakes a role acting like a proton shuttle and/or as a valve in the area for the flow of protons towards Cu_B/Fe_{a3} and prop-D/Arg salt bridge [26,27]. Prop-D/Arg salt bridge has been proposed to be in a redox-dependent thermal equilibrium, acting as a gate for a proton or a protonated water molecule [22]. As discussed in a previous study [21] the Cu_B position is extremely sensitive to the protonation states of the propionates. This thermal equilibrium and proton transient gate should alter Fe_{a3}–Cu_B distance that might trigger vibrational resonances in the His–Fe^{IV}=O ferryl moiety of the active site, exerted as different bands in the resonance Raman spectra [20].

B. Water molecules are possible sites for the accommodation of a proton in the form of transient hydronium (H_3O^+) species, acting as proton carriers. Interestingly enough, a single water molecule is highly conserved in the crystal structures of bacterial and mammalian CcO, between the heme a_3 propionates. If such a hydronium molecule is interacting with the protein matrix in the area of the heme a_3 propionates, its proton is transferred to the heme a_3 ring A propionate in QM/MM simulations. This implicates a prop-D/Arg → prop-A/Asp399 proton transfer via the conserved water molecule in the cases where a single proton is shared between prop-A and Asp399 [21].

C. The protonation of prop-A/Asp399 via the D-proton pathway controls the His403 conformation. The protonation enables the neutralization of the prop-A/Asp399 pair, while the His403 conformation changes to facilitate the easy transfer of the extra proton to the water pool and the solvent [21]. The His403 residue plays a role, as a valve, controlling the flow of protons in the region. By substantially changing the pK_a values of the prop-A or Asp399, a proton is trapped

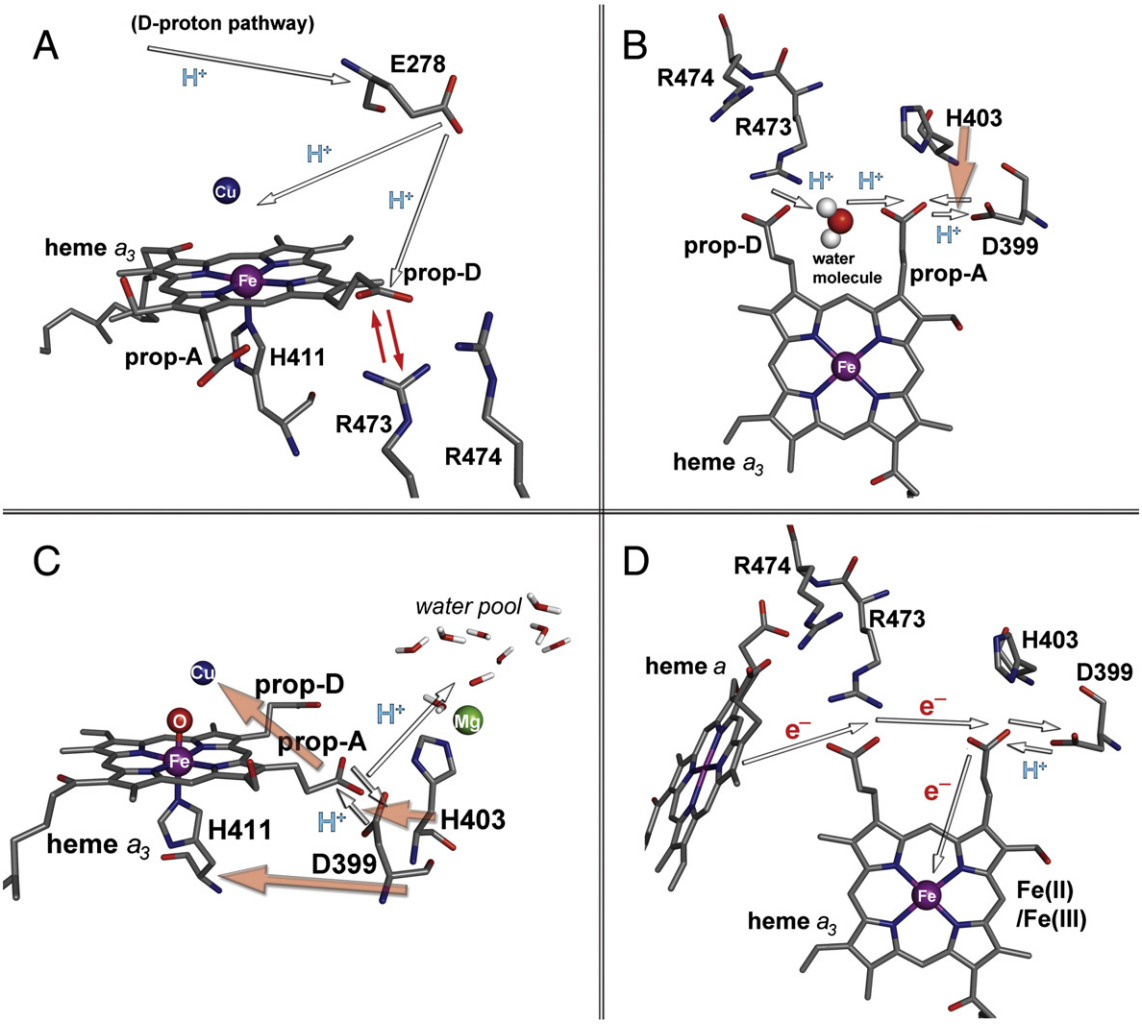

Fig. 3. Schematic overview of the proposed electron/proton coupled mechanism of action in cytochrome *c* oxidase dioxygen reaction. A. A proton is coming from E278 and the D-pathway, via the prop-D/Arg473 gate. E278 delivers protons to the Cu_B and/or the prop-D/Arg473 site. B. The proton is transferred to the prop-A/Asp399 pair with the involvement of a water molecule in equilibrium in-between the heme a_3 propionates. This neutralizes the charges on the prop-A/Asp399 pair and His403 controls its protonation state. This affects the intensities of the ν(Fe–O)/δ(His–Fe=O) vibrational frequencies and alters the His403 conformation to enable the release of that proton. C. His403 can convert a rather stable carboxylic proton between prop-A/Asp399 to a more acidic one, while the latter pair accepts a second proton. His403 residue is involved in the controlling of the protonation states of the prop-A/Asp399 pair, and the release of protons out of the active site. The protonation state of the prop-A/Asp399 pair controls the Cu_B position, while effects in the proximal area are also communicated by the prop-A/Asp399/ His403 triad. D. The proton release is controlled by the oxidation state of the heme a_3/Cu_B active site, as it appears "blocked" in the case of the oxy-Fe^{II}/Cu_B^{II} intermediate, while half spin can be allocated in the propionates area coupling electron/proton motion in the prop-A/Asp399 pair.

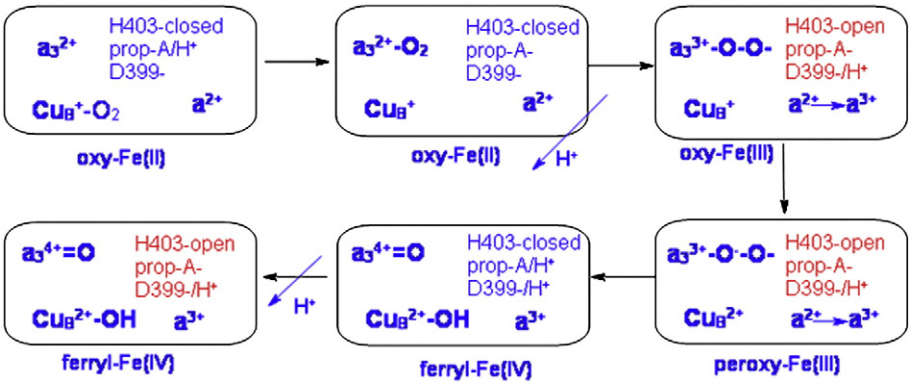

Fig. 4. Proposed mechanism of action involving the His403 conformational change to control the protonation state of the prop-A/Asp399 pair. His403 closed conformation enables the release of a proton out of the active site in all the cases except the oxy (Fe^{II}) intermediate.

or released by prop-A. When His403 is at the closed conformation (strong hydrogen bonding with Asp399) the proton is in the majority of the cases loosely bound on the carboxylic groups of prop-A/Asp399 (oxy intermediate is the only exception) [21]. Moreover, in the case of the ferryl intermediate of the CcO/dioxygen reaction, different protonation states of the prop-A/Asp399 pair are able to control the intensities of the ν(Fe–O) bands [19]. His403 and Asp399 are few amino acids apart in the same chain sequence from the Gly386/Thr389. Thus, protonation/ deprotonation events in the prop-A/Asp399 pair, as well as the His403 conformational changes are communicated via this chain to the proximal site of His411. Differentiations in the hydrogen bonding strengths in the proximal region (see Fig. 5) are able to control the His411 basicity and thus the ν(Fe–O) modes via resonances [20]. On this line, it should be mentioned that it has been proposed by Kitagawa that in the presence of an electron-withdrawing group attached to heme a_3 (formyl), the a_{1u} and a_{2u} level could be lower than the d_{xz} and d_{yz} orbitals [28]. Thus, an electron is taken out of the iron orbital, producing the Fe(V) oxidation state, and the d_{xz} and d_{yz} orbitals may act as antibonding orbitals of the Fe(V) = O bond. Consequently, removal of this electron raises the stretching frequency of the Fe(V) = O as compared with the Fe(IV) = O frequency.

D. His403 controls the pK_a values of the prop-A/Asp399 pair. Starting from a structure where a single proton is shared between the latter pair, in the oxy intermediate, and the closed His403 conformation, the proton resides 'locked' on the prop-A side. Active site oxidation will trigger the release of that proton as it becomes loosely bound (between prop-A/Asp399) in the rest of the oxidation states and the His403 closed conformation. A water molecule in the area could easily abstract the labile proton. The prop-A/Asp399 pair becomes fully deprotonated. Deprotonation of the prop-A/Asp399 pair increases the presence of negative charges in the area, reallocating Cu_B closer to heme a_3 iron, accommodating also half spin in prop-A. Heme a_3 is oxidized Fe(II) → Fe(III) upon protonation of the prop-A/Asp399 pair via the D-pathway [21]. Electron transfer

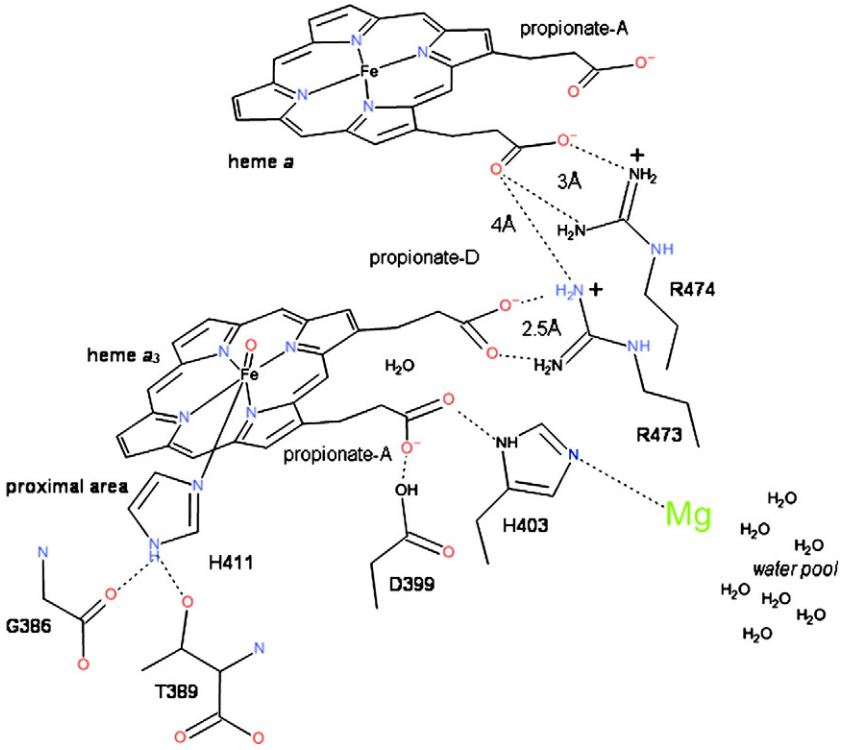

Fig. 5. Protonic connectivity between the heme *a* and heme a_3 propionates and the conserved residues His411/G386–T389 and the heme a_3–propionateA–D399–H403 chain.

should occur from heme *a*, concurrently to the previous proton transfer to quench the half spin population on prop-A. This should eventually trigger cycles of the further oxidation of the active site to the peroxy and ferryl intermediates. Protonation should change the His403 conformation as discussed previously, in this case trapping the proton on the Asp399 site (His403 open conformation). Another release of a proton to the propionates area via the D-pathway is able to neutralize the prop-A/Asp399 charges and protons become loosely attached to the pair, in this way (His403 closed conformation). A water molecule out of the active site can be a possible proton carrier, as well as a trigger for the neutralization of the prop-A/Asp399 pair and the His403 conformational change. In each case, a loosely bound carboxylic proton residing on prop-A/Asp399 is released to the water pool and later or immediately to the solvent when His403 changes conformation from open to closed. The change of His conformation from open to closed indicates a proton release out of the active site, but not necessarily a proton pump to the solvent. The mechanism described is shown in Fig. 4.

4. Conclusions

We propose a mechanism in which the coupling of the oxygen reduction chemistry to proton translocation (P→F transition) is related to the properties of two groups of conserved residues, namely, His411/G386–T389 and the heme a_3–propionateA–D399–H403 chain (Fig. 5). In addition, we have linked significant intermediates of the proton pumping mechanism to spectroscopic characteristics and we have discussed proton/electron coupling in CcO/dioxygen reaction, based on QM, MD and QM/MM calculations. We propose that during the enzymatic turnover, a proton coming from E278 and the D-pathway, via the prop-D/Arg473 gate [22] neutralizes the prop-A/Asp399 charges with the involvement of a water molecule in equilibrium with the prop-A/Asp399 pair [21]. This affects the intensities of the ν(Fe–O)/δ(His–Fe=O) vibrational frequencies and alters the His403 conformation to enable the release of that proton. This is achieved by the conversion of a rather stable carboxylic proton between prop-A/Asp399 to a more acidic one, while the latter pair accepts a second proton. His403 residue is involved in the controlling of the protonation states of the prop-A/Asp399 pair, and the release of protons out of the active site (Fig. 5). It seems that this proton release is also controlled by the oxidation state of the heme a_3/Cu_B active site, as it appears "blocked" in the case of the oxy-Fe^{II}/Cu_B intermediate [21].

Acknowledgements

We thank Prof. Ludwig for the samples of aa_3 oxidase from *P. denitrificans*. This work was supported by funds from the Cyprus Research Promotion Foundation to C.V (TEXNOLOGIA/THEPIS/0609(BE)/05) and to EP (ANAVATHMISI/PAGIO/0308/14).

References

[1] S. Ferguson-Miller, G.T. Babcock, Heme–copper terminal oxidases, Chem. Rev. 7 (1996) 2889–2907.
[2] M. Wikstrom, M.I. Verkhovsky, Mechanism and energetic of proton translocation by the respiratory heme–copper oxidases, Biochim. Biophys. Acta 1767 (2007) 1200–1214.
[3] P. Brzezinski, R.B. Gennis, Cytochrome *c* oxidase: exciting progress and remaining mysteries, J. Bioenerg. Biomembr. 40 (2008) 521–531.
[4] S. Han, Y.-C. Ching, D.L. Rousseau, Ferryl and hydroxy intermediates in the reaction of oxygen with reduced cytochrome *c* oxidase, Nature 348 (1990) 89–90.
[5] T. Ogura, S. Takahashi, K. Shinzawa-Itoh, S. Yoshikawa, T. Kitagawa, Observation of the iron(II)–oxygen stretching Raman band for cytochrome oxidase compound A at ambient temperature, J. Am. Chem. Soc. 112 (1990) 5630–5631.
[6] C. Varotsis, W.H. Woodruff, G.T. Babcock, Direct detection of a dioxygen adduct of cytochrome a_3 in the mixed valence cytochrome oxidase/dioxygen reaction, J. Biol. Chem. 265 (1990) 11131–11136.
[7] C. Varotsis, G.T. Babcock, Appearance of the $\nu(Fe^{IV}=O)$ vibration from a ferryl–oxo intermediate in the cytochrome oxidase/dioxygen reaction, Biochemistry 29 (1990) 7357–7362.
[8] D.A. Proshlyakov, T. Ogura, K. Shinzawa-Itoh, S. Yoshikawa, T. Kitagawa, Microcirculating system for simultaneous determination of Raman and absorption spectra of enzymatic reaction intermediates and its application to the reaction of cytochrome *c* oxidase with hydrogen peroxide, Biochemistry 35 (1996) 76–82.
[9] E. Pinakoulaki, U. Pfitzner, B. Ludwig, C. Varotsis, Direct detection of Fe(IV)=O intermediates in the cytochrome aa_3 oxidase from *Paracoccus denitrificans*/H_2O_2 reaction, J. Biol. Chem. 278 (2003) 18761–18766.
[10] W.A. Oertling, H. Hoogland, G.T. Babcock, R. Wever, Identification and properties of an oxoferryl structure in myeloperoxidase compound II, Biochemistry 27 (1988) 5395–5400.
[11] C. Varotsis, M. Vamvouka, Resonance Raman and FTIR studies of carbon monoxide-bound cytochrome aa_3-600 oxidase of *Bacillus subtilis*, J. Phys. Chem. B 102 (1998) 7670–7673.
[12] T.L. Poulos, Heme enzyme crystal structures, Adv. Inorg. Biochem. 7 (1988) 1–36.
[13] J.H. Dawson, Probing structure–function relations in heme-containing oxygenases and peroxidases, Science 240 (1988) 433–439.
[14] W.A. Oertling, R.T. Kean, R. Wever, G.T. Babcock, Factors affecting the iron–oxygen vibrations of ferrous oxy and ferryl oxo heme proteins and model compounds, Inorg. Chem. 29 (1990) 2633–2645.
[15] C. Koutsoupakis, T. Soulimane, C. Varotsis, Probing the Q-proton pathway of ba_3_cytochrome *c* oxidase by time-resolved Fourier transform infrared spectroscopy, Biophys. J. 86 (2004) 2438–2444.
[16] T. Ohta, E. Pinakoulaki, T. Soulimane, T. Kitagawa, C. Varotsis, Detection of a photostable five-coordinate heme a_3–Fe–CO species and functional implications of His384/α10 in CO-bound ba_3–cytochrome *c* oxidase from *Thermus thermophilus*, J. Phys. Chem. B 108 (2004) 5489–5491.
[17] E. Pinakoulaki, T. Ohta, T. Soulimane, T. Kitagawa, C. Varotsis, Simultaneous resonance Raman detection of the heme a_3–Fe–CO and Cu_B–CO species in CO-bound ba_3–cytochrome *c* oxidase from *Thermus thermophilus*: evidence for a charge transfer Cu_B–CO transition, J. Biol. Chem. 279 (2004) 22791–22794.
[18] I. Bellevich, M.I. Verkhovsky, M. Wikstrom, Proton-coupled electron transfer drives the proton pump of cytochrome *c* oxidase, Nature 440 (2006) 829–832.
[19] V. Daskalakis, S.C. Farantos, C. Varotsis, Assigning vibrational spectra of ferryl–oxo intermediates of cytochrome *c* oxidase by periodic orbits and molecular dynamics, J. Am. Chem. Soc. 130 (2008) 12385–12393.
[20] V. Daskalakis, S.C. Farantos, V. Guallar, C. Varotsis, Vibrational resonances and Cu_B displacement controlled by proton motion in cytochrome *c* oxidase, J. Phys. Chem. B 114 (2010) 1136–1143.
[21] V. Daskalakis, S.C. Farantos, V. Guallar, C. Varotsis, Regulation of electron and proton transfer by the protein matrix of cytochrome *c* oxidase, J. Phys. Chem. B 115 (2011) 3648–3655.
[22] M. Wikstrom, C. Ribacka, M. Molin, L. Laakkonen, M. Verkhovsky, A. Puustinen, Gating of proton and water transfer in the respiratory enzyme cytochrome *c* oxidase, Proc. Natl Acad Sci. USA 102 (2005) 10478–10481.
[23] U. Pfitzner, A. Odenwald, T. Ostermann, L. Weingard, B. Ludwig, O.-M.H. Richter, Cytochrome *c* oxidase from *Paracoccus denitrificans* analysis of mutations in putative proton channels of subunit I, J. Bioenerg. Biomembr. 30 (1998) 89–97.
[24] X. Zheng, D.M. Medvedev, J. Swanson, A.A. Stuchebrukhov, Computer simulations of internal water in cytochrome oxidase, Biochim. Biophys. Acta 1557 (2003) 99–107.
[25] A. Puustinen, J.A. Bailey, R.B. Dyer, S.L. Mecklenburg, M. Wikstrom, W.H. Woodruff, Fourier transform infrared evidence for connectivity between Cu_B and glutamic acid 286 in cytochrome bo_3 from *E. coli*, Biochemistry 36 (1997) 13195–13200.
[26] E. Olkhova, C. Hutter, M.A. Lill, V. Helms, H. Michel, Possible water networks in cytochrome *c* oxidase from *Paracoccus denitrificans* investigated by molecular dynamics simulations, Biophys. J. 86 (2004) 1873–1889.
[27] J. Xu, G.A. Voth, Redox-coupled proton pumping in cytochrome *c* oxidase: further insights from computer simulation, Proc. Natl Acad Sci. USA 102 (2005) 6795–6800.
[28] T. Kitagawa, Structure of reaction intermediates of bovine cytochrome *c* oxidase probed by time-resolved vibrational spectroscopy, J. Inorg. Biochem. 82 (2000) 9–18.